Unintended filtering in a typical photodiode detection system for optical tweezers

Kirstine Berg-Sørensen and Lene OddershedeErnst-Ludwig FlorinHenrik Flyvbjerg

Citation: **93**, 3167 (2003); doi: 10.1063/1.1554755
View online: http://dx.doi.org/10.1063/1.1554755
View Table of Contents: http://aip.scitation.org/toc/jap/93/6
Published by the American Institute of Physics

Unintended filtering in a typical photodiode detection system for optical tweezers

Kirstine Berg-Sørensen[a] and Lene Oddershede
The Niels Bohr Institute, Blegdamsvej 17, DK-2100 Copenhagen Ø, Denmark

Ernst-Ludwig Florin
European Molecular Biology Laboratory, Heidelberg, Germany

Henrik Flyvbjerg
Materials Research Department, Risø National Laboratory, DK-4000 Roskilde, Denmark

(Received 28 October 2002; accepted 20 December 2002)

We characterize the frequency-dependent response of a photo detection system based on a Si-PIN photodiode and a laser with wavelength 1064 nm, a system commonly used with optical tweezers. We chopped the laser beam with chopper frequencies from 200 Hz to 14 kHz, and found an exponentially delayed response of the detection system with a characteristic delay time of $\sim 20\,\mu$s. The physical mechanism causing this time delay is silicon's transparency to 1064 nm light: Photons are absorbed and create charge carriers not only in the diode's depletion layer, where they are detected within nano-seconds, but predominantly in the *n*-layer, where they remain undetected till transported out by thermal diffusion. The diode's response is dominated by this delay which can be characterized as a first-order low-pass filter with a 3dB-frequency of 8–9 kHz, depending on laser intensity. Measurements exploiting frequencies near or above this 3dB-frequency must be corrected for this unintended filter effect. We describe how to do this, and how to diagnose other systems which may or may not have the same problem. Explanations are intended for users of photo detection systems, and present the little semi-conductor physics needed to make sense. © *2003 American Institute of Physics.* [DOI: 10.1063/1.1554755]

I. INTRODUCTION

Photodiode based detection systems are used in a number of modern techniques, ranging from detection of the position of the laser beam in atomic force microscopes,[1,2] over detection schemes of optical tweezers (Refs. 3, and 4, and references therein), to equipment used in high-energy physics particle detectors.[5,6] In some cutting-edge biological applications, optical tweezers are used as very sensitive force transducers.[7–14] When used in this capacity, it is crucial to have a precise calibration of the trap. It consequently caused concern when a significant unexplained power-loss was noted in the power spectrum of the motion of a free bead in a trap, in the frequency-range above the trap's corner frequency.[15] Similar observations were made in[9,16] where consequently only low-frequency data were used.

This ''mysterious'' power-loss is investigated experimentally, explained physically, and modeled quantitatively here. Consequently, one can compensate for it by calibration, and in this manner increase the reliable part of the power spectrum significantly.

The experiment is simple: the photodetection system is given an input of fixed, known frequency by chopping the laser beam with a beam chopper. We record and study the detection system's response as function of chopper frequency.

The response is surprisingly simple. It is a sum of two terms: an ''instantaneous'' response within nanoseconds, as intended by design, but with reduced amplitude, *plus* an exponential tail of delayed response with a decay time $\tau \approx 20\,\mu$s. In the frequency domain, this response is that of a first-order filter with 3dB-frequency $f_{3\mathrm{dB}} = (2\pi\tau)^{-1} \approx 8$ kHz.

As one might expect from the simple response, its physical explanation is equally simple: Silicon, the material from which the diode was made, is almost transparent at the laser wavelength used for biological reasons. Consequently, light is absorbed both in the diode's depletion region, as intended, and in the *n*-layer behind the depletion layer. The electron–hole pairs thus created in the depletion layer's conduction/valence band are separated within nanoseconds by that layer's electrical field, ''instantaneously'' creating the voltage we record. The valence holes created in the field-free *n*-layer, on the other hand, must first diffuse into the depletion layer before they are separated from the conduction electrons they were created with, and consequently cause a delayed signal.

The simplest possible model based on this physical scenario turns out to be all that is needed for a precise quantitative description of the recorded signals. Consequently, the filter characteristics of the photodetection system is a simple analytical function. This is fortunate, because the power loss diagnosed here depends on the intensity of the laser light, hence must be recalibrated each time the detection system is used, as described for the case of optical tweezers in Ref. 15.

[a]Author to whom correspondence should be addressed; electronic mail: berg@nbi.dk

This calibration is possible because the filter characteristics is simple.

The detection system analyzed here is quite common, and similar to the one used in Refs. 9, 10 and 16–22. We emphasize that nothing is wrong with the photodiode as such. It is just not performing well with infrared light. Infrared light is a natural choice for tweezers on biological grounds. Silicon is a natural choice for diode material on physical grounds. It is the laser/diode mismatch that causes the problem, and there is no clue to this problem in the diode's specifications:

The diode's spectral response range is 320–1100 nm, with peak sensitivity at 960 nm.[23] At 1064 nm, the wavelength of our laser, the diode's sensitivity is half its peak value, hence quite acceptable. The diode's frequency response is given as a cutoff frequency $f_{\text{cutoff}}=20$ MHz measured at 10 V reverse bias and 50 Ω load, corresponding to a rise time $\tau_{\text{rise}}=(\ln 9)/(2\pi f_{\text{cutoff}})=17$ ns.[23] This rise time is equivalent to a characteristic time $\tau=1/(2\pi f_{\text{cutoff}})=8$ ns for the exponential saturation of output that the definition of rise time refers to.[24] The wavelength at which this cutoff frequency was measured, is not given on the data sheet, but a catalogue containing similar, slightly older, diodes[24] gives two wavelengths: 560 and 655 nm. So one does not know the cutoff frequency for 1064 nm light. Neither does one know the cutoff frequency at zero reverse bias, but the data sheet gives the terminal capacitance versus reverse voltage, and the terminal capacitance is the major factor in determining the response speed of the photodiode. It increases by a factor 5 only, when the reverse voltage is decreased from 10 to 0.1 V, and its trend is toward *less* voltage dependence at lower voltages. It is not given below 0.1 V.

None of this contains a clue to the results we present below: characteristic times 2500-fold larger than the 8 ns given above. On the contrary, with a factor 5 or so increase in terminal capacitance, one would still expect a cutoff frequency on the order of MHz.

The section on frequency response in Ref. 24 does, however, mention charge carriers generated outside the depletion layer, and that their diffusion time ''may sometimes be greater than several microseconds.'' With our diode, zero reverse bias voltage, and 1064 nm light, this is the case, and a serious problem because *most* charge carriers are generated outside the depletion layer: The width of the depletion layer is minimal when there is no reverse bias. That leaves a field-free zone of maximal size behind the depletion layer. This in itself is no problem, if most light is absorbed in the depletion layer. As already mentioned, however, silicon is almost transparent to the 1064 nm light we use. Combined with the minimal depletion layer, this results in a signal that is dominated by holes generated in the *n*-layer. They give rise to a delayed part in the total signal, while its instantaneous part, caused by charge carriers generated in the depletion layer, is subdominant. The power spectrum is a function of signal amplitude *squared*, so when the instantaneous part of the signal is small, its contribution to the power spectrum is small to second order, thus magnifying the importance of the delay.

This subtle interplay between several effects, none of which are problems by themselves, is probably the reason why the problem could arise in the first place, and remain unexplained for awhile.

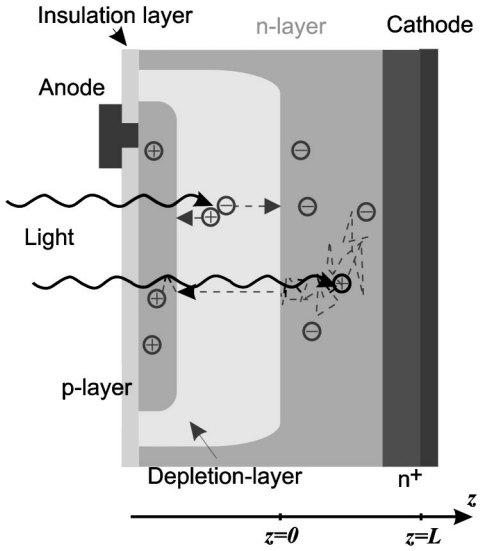

FIG. 1. Typical construction of a photodiode, as seen from the side in cross section. Reproduced from Ref. 24. Not to scale. The diode is 320 μm thick from anode to cathode. The *p*-layer is about 1 μm thick or less. At zero reverse bias voltage, the depletion layer is 12 μm thick, at 15 V reverse bias it is 70 μm thick (see Ref. 29).

II. EXPERIMENTS

Light from a Spectra Physics Millenia Nd:YVO_4 laser lasing with constant intensity at a wavelength of 1064 nm was chopped with constant frequency by a mechanical chopper. This was repeated for a number of chopper frequencies in the range 200 Hz–14 kHz. The chopper wheel made by our local machine shop has $n_{\text{hole}}=120$ holes, and a radius of 47 mm measured from the center of the wheel to the centers of the holes. The hole size is 1.4 mm in the angular direction and 2.2 mm in the radial direction, with straight, radially aligned sides leaving 1.5 mm between the holes at radius 47 mm. The laser beam has a Gaussian intensity profile. The chopper was positioned in the focus plane between two lenses to ensure a beam waist much smaller than the size of the chopper holes. Laser and chopper were aligned such that the beam passes through the centers of the chopper holes.

The quadrant photodiode is a Hamamatsu S5981 Si-PIN diode (see Fig. 1.) operated with no reversed bias voltage for reasons we shall return to. The signal reported is the total intensity, i.e., the sum of the voltages recorded by the four quadrants. From the diode, the signal is fed through a preamplifier and an amplifier before analog-to-digital conversion (ADC) and recording by PC through LABVIEW software. The preamplifier was built by Wolfgang Öffner (EMBL-Heidelberg) and has a gain of 20 kV/A, and a built-in first-order filter with nominal 3dB-frequency $f_{3\text{dB}}=80$ kHz. We confirmed this frequency in a separate measurement, using a red light-emitting diode as the light source, since it suffers no power loss in the photodiode. In the amplifier the data were low-pass filtered with a first-order filter with $f_{3\text{dB}}=50$ kHz.

By feeding a periodic signal from a function generator directly into the amplifier, we confirmed that the characteristics of this filter is that of a first-order filter

$$\frac{P(f)}{P_0(f)} = \frac{1}{1+(f/f_{3\mathrm{dB}})^2}. \tag{1}$$

The ADC card (PCI-MIO-16E-4, National Instruments) did not cause discernible filtering.

These tests ensure that the effect reported here is caused by the photodiode and preamplifier alone. Since it is not possible to measure their individual characteristics, and also not necessary because they work together in all photodetection systems, only their combined characteristics are reported here. Nevertheless, we expect the effect to arise from the photodiode.

III. PHYSICAL MODEL

The Si-PIN photodiode is constructed as illustrated in Fig. 1. Valence electrons are excited to the conduction band when photons are absorbed, leaving holes in the valence band. When these charge carriers are created in the depletion layer, the electrical field there separates them in nanoseconds. This gives rise to a voltage one records, and is the intended response of the photodiode.

At the 1064 nm wavelength used, silicon has an absorption coefficient of less than $1\ \mathrm{cm}^{-1}$ at 300 K. Doping increases absorption, but not by orders of magnitude.[25] Consequently, little laser light is absorbed, so the little that is, is absorbed in equal amounts at all depths z of the diode; in the depletion layer, as intended; in the *p*-layer, which is so thin by design that it can be ignored; and in the *n*-layer. The *n*-layer is field free, i.e., has constant electrical potential. This potential drops across the depletion layer to a lower constant value in the *p*-layer, which is also field free (Ref. 26, Fig. 29.4). Consequently, conduction electrons and valence holes created in the *p*- and *n*-layers move only by thermal diffusion. When holes diffusing in the *n*-layer reach the depletion layer, the electrical field there pulls them across the layer in nanoseconds, building a voltage that is delayed with respect to its cause. Conduction band electrons created in the *p*-layer contribute to this voltage when they diffuse to the depletion layer, but since the *p*-layer is so much thinner than the *n*-layer, they arrive much sooner, and in much smaller numbers. Their contribution to the recorded voltage effectively appears with that from the depletion layer. For this reason, only diffusion of holes in the *n*-layer are used to model the delayed part of the diode's output.

The time delay with which these holes give rise to a current is governed by their diffusive motion along the z-axis (see Fig. 1). Diffusion in directions orthogonal to the z-axis takes place simultaneously, independently, but does not affect diffusion in the z direction. So one can integrate over the two orthogonal coordinates, and work with the resulting density $\rho(z,t)$ of holes as function of depth z within the *n*-layer. The time evolution of this density is governed by the diffusion equation

$$\frac{\partial\rho}{\partial t} = \mathcal{D}\frac{\partial^2\rho}{\partial z^2}, \tag{2}$$

where D is the thermal diffusion coefficient of holes. In pure silicon, $\mathcal{D}=12.9\ \mathrm{cm}^2/\mathrm{s}$ at room temperature, and it decreases to one tenth of this value with increasing impurity concentration (Ref. 27, Fig. 4.11). In the low-doped *n*-layer, D's value in pure silicon is a good approximation (Ref. 27, Fig. 4.11), (Ref. 5, Example 5.1), which will be used throughout this article.

Equation (2) ignores the disappearance of holes through recombination with conduction electrons. This approximation is good to about 2% because the mean lifetime before a diffusing hole disappears by recombination in a lowly doped *n*-layer is of order 1 ms (Ref. 5, Example 5.1), while we shall find that a diffusing hole disappears by detection within a mean time of 20 μs.

The *n*-layer's boundaries are located at $z=0$ and $z=L$ (see Fig. 1). The boundary to the depletion layer at $z=0$ is absorbing, while the boundary to the cathode at $z=L$ is reflecting, i.e.,

$$\rho(z=0,t)=0, \quad \frac{\partial\rho}{\partial z}(z=L,t)=0. \tag{3}$$

The details of this simple scenario may not be strictly correct. The boundary at L may be partly absorbing, e.g., Ref. 5, p. 97, depending on details not available to us. The scenario defines a specific, easily solvable case, however, and yields results which qualitatively are valid in general. The solution to the diffusion equation in *any* compact volume, e.g., can be written as a discrete sum of eigenmodes, each with its own relaxation time. If this volume has an absorbing boundary, as here, the current out of the volume consequently decreases exponentially with time at late times, as found below.

Since detection is rapid once a hole has reached the depletion layer, the delayed part of the signal is given by the diffusive current of holes out of the *n*-layer and into the depletion layer. This current $I(t)$ is given by Fick's law

$$I(t) = -\mathcal{D}\frac{\partial\rho}{\partial z}(z=0,t). \tag{4}$$

The general solution $\rho(z,t)$ to Eqs. (2) and (3) is a linear combination of a complete set of orthogonal solutions found by Fourier analysis

$$\rho(z,t) = \sum_{n=0}^{\infty} b_n \exp(-t/\tau_n)\sin\left(\frac{(2n+1)\pi}{2}\frac{z}{L}\right), \tag{5}$$

where the characteristic decay time τ_n of the nth spatial mode is

$$\tau_n = \mathcal{D}^{-1}\left(\frac{2L}{(2n+1)\pi}\right)^2. \tag{6}$$

The decay times decrease rapidly with n, the longest time constant being

$$\tau_0 = \frac{4L^2}{\pi^2\mathcal{D}}, \tag{7}$$

and the following being factors 9, 25, 49, 81,...shorter. Since the diode is effectively transparent, the initial density of holes created by a flash of light is uniform, $\rho(z, t=0) = \rho_0$. Consequently,

$$b_n = \frac{4\rho_0}{(2n+1)\pi}, \tag{8}$$

which gives the slowest mode the largest amplitude, three times larger, e.g., than the next-largest amplitude, that of the next slowest mode.

The diffusive current of holes $I(t)$ out of the n-layer is

$$I(t) = \frac{\pi\mathcal{D}}{2L}\sum_{n=0}^{\infty}(2n+1)b_n \exp(-t/\tau_n)$$

$$= \frac{2\rho_0\mathcal{D}}{L}\sum_{n=0}^{\infty}\exp(-t/\tau_n), \tag{9}$$

where the last identity assumes a constant initial density. With $\tau_0 \approx 20\,\mu$s, as reported below, and $\mathcal{D} = 12.9\,\mathrm{cm}^2/\mathrm{s}$, $L = 250\,\mu$m, in reasonable agreement with Fig. 1.

Anticipating the result $\tau_0 \approx 20\,\mu$s, we find $\tau_1 \approx 2\,\mu$s. For comparison, the time constant of the amplifier's low-pass filter is approximately 3 μs. Consequently, all decay modes that are faster than the slowest one merge with the instantaneous diode response, while only the slowest mode is well resolved. We assume this is correct, and find below that the consequences of this assumption fit our data perfectly.

The first consequence is that the response function $g(t)$ of the photodiode can be modeled with just two terms

$$g(t) = \alpha^{(\mathrm{diode})}\delta(t) + (1-\alpha^{(\mathrm{diode})})\frac{1}{\tau}\exp\left(-\frac{t}{\tau}\right), \tag{10}$$

where $\alpha^{(\mathrm{diode})}$ is the fraction of effectively instantaneous response, and the time t is the time interval from when a pulse of light hits the diode until it is recorded. We see that any pulse of light will be recorded at all later times due to the exponential in Eq. (10). Specifically, a generic signal $S(t)$ will be recorded as a superpositon of itself, recorded with different delays, and weighted accordingly

$$S^{(\mathrm{del})}(t) = \int_{-\infty}^{t} dt' g(t-t')S(t') = (g*S)(t), \tag{11}$$

where the asterix denotes convolution of functions, and ''del'' is short for ''delayed.''

It is a puzzling fact that it is because the photodiode so thoroughly *fails* to absorb photons that we can easily compensate for this by calibration. This failure ensures a spatially constant initial density of the holes created by a flash of light. It is this initial density that makes the slowest eigenmode of the diffusion equation so entirely dominated by the detected delay.

The value of $\alpha^{(\mathrm{diode})}$ is related to diode dimensions. Let $L^{(\mathrm{dep})}$ denote the width of the depletion layer. Then a flash of light produces $\rho_0 L^{(\mathrm{dep})}$ holes in the depletion layer, and $\rho_0 L$ holes in the n-layer. The latter holes can be divided into those detected with the distribution of delays characteristic of the slowest eigenmode of the diffusion equation, and those detected as belonging to faster modes. Equation (9) already contains this division. By integrating the first term in its sum over time from 0 to ∞, we find that $(8/\pi^2)\rho_0 L$ holes arrive with the delay of the slowest mode. The rest of the holes created in the n-layer, $(1-8/\pi^2)\rho_0 L$ of them, are detected instantaneously with our time resolution, i.e., simultanously with the holes created in the depletion layer. Consequently,

$$\alpha^{(\mathrm{diode})} = \frac{\rho_0 L^{(\mathrm{dep})} + \rho_0 L(1-8/\pi^2)}{\rho_0 L^{(\mathrm{dep})} + \rho_0 L}$$

$$= 1 - \frac{8/\pi^2}{1 + L^{(\mathrm{dep})}/L}. \tag{12}$$

In the limit $L^{(\mathrm{dep})}/L \to 0$, $\alpha^{(\mathrm{diode})}$ takes its smallest possible value, $1-8/\pi^2 = 0.19$, and only for $L^{(\mathrm{dep})} \gg L$ is $\alpha^{(\mathrm{diode})} \approx 1$ for an almost transparent photodiode.

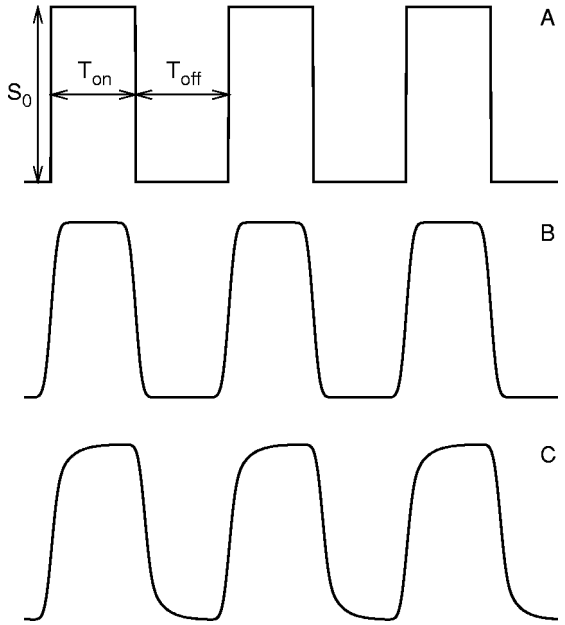

FIG. 2. Sketch of model for recorded signal. (A) Train of rectangular pulses $S^{(\mathrm{rect})}(t)$, the signal from a chopped, infinitely narrow, laser beam impinging on a diode with instantaneous response. (B) Train of pulses $S^{(\mathrm{erf})}(t)$ produced by chopping a laser beam with finite waist and Gaussian profile, impinging on a diode with instantaneous response. (C) Train of pulses $S^{(\mathrm{erf,del})}(t)$ produced as in B, but recorded with a diode with an exponentially delayed response.

IV. TIME SERIES: MODELS

In this section, we model the time series recorded by the photodiode detection system when a laser beam is chopped. Readers uninterested in mathematical details can skip this section.

The model is sketched in Fig. 2. First, assume signals are recorded without delay, and the beam waist is infinitely narrow. Chopping such a beam produces a signal that is a train of rectangular pulses [see Fig. 2(A)]. Parametrized by height S_0, on-time T_{on}, and off-time T_{off}, the signal can be written

$$S^{(\mathrm{rect})}(t) = S_0 \sum_n \{\Theta(t_n) - \Theta(t_n - T_{\mathrm{on}})\}, \tag{13}$$

where

$$t_n \equiv t - t_0 + nT = t - t_{0,n}. \tag{14}$$

Here t_0 defines the phase and $T \equiv T_{\text{on}} + T_{\text{off}}$ is the period of the signal.

The laser beam is not infinitely narrow, however. It has a Gaussian profile with a small, but finite beam waist σ_x. The angle extended by one hole of the chopper is $\sim 1.5°$ of arc. Therefore, the motion of the edge of a hole across the beam is well approximated by a straight-edged shutter moving rectilinearly across the beam. Thus chopping this beam replaces the Θ function in Eq. (13) with

$$\begin{aligned}\Theta(t) \to \Theta^{(\text{erf})}(t) &= \frac{S_0}{2\pi\sigma_x^2}\int_{-\infty}^{r\omega t}\int_{-\infty}^{\infty}\exp\left(-\frac{x^2+y^2}{2\sigma_x^2}\right)dx\,dy \\ &= \frac{S_0}{\sqrt{2\pi\sigma_x^2}}\int_{-\infty}^{r\omega t}\exp\left(-\frac{x^2}{2\sigma_x^2}\right)dx \\ &= \frac{S_0}{2}\left[1+\text{erf}\left(\frac{t}{\sqrt{2\sigma_t}}\right)\right],\end{aligned} \tag{15}$$

i.e., a ''smoothed'' step function. Here, the integral in the first identity has the *y*-axis parallel to the shutter's edge and the *x*-axis in the shutter's direction of motion. Also, we have introduced $\sigma_t = \sigma_x/(r\omega)$, which is the time it takes for the shutter edge to cover the distance σ_x, and ω, the cyclic frequency of the wheel, which is related to the chopper frequency f_{chop} by $f_{\text{chop}} = n_{\text{hole}}\omega/2\pi$.

Thus, if signals were recorded without delay, the signal from a chopped Gaussian beam with finite waist is

$$S^{(\text{erf})}(t) = \frac{S_0}{2}\sum_n\left\{\text{erf}\left(\frac{t_n}{\sqrt{2\sigma_t}}\right) - \text{erf}\left(\frac{t_n - T_{\text{on}}}{\sqrt{2\sigma_t}}\right)\right\}. \tag{16}$$

The graph of $S^{(\text{erf})}(t)$ is shown in Fig. 2(B).

Next, we take into account the finite response time of the diode as modeled in Eq. (10), and find

$$\begin{aligned}\Theta^{(\text{erf})}(t) \to \Theta^{(\text{erf,del})}(t) &= (g * \Theta^{(\text{erf})})(t) \\ &= \frac{S_0}{2}\left\{\text{erf}\left(\frac{t}{\sqrt{2\sigma_t}}\right) - (1-\alpha^{(\text{diode})})\exp\left(\frac{\sigma_t^2}{2\tau^2}\right)\right. \\ &\quad \left.\times\exp(-t/\tau)\left[1+\text{erf}\left(\frac{t}{\sqrt{2\sigma_t}} - \frac{\sigma_t}{\sqrt{2\tau}}\right)\right]\right\},\end{aligned} \tag{17}$$

hence

$$\begin{aligned}S^{(\text{erf,del})}(t) &= (g * S^{(\text{erf})})(t) \\ &= \sum_n\left[\Theta^{(\text{erf,del})}(t_n) + \Theta^{(\text{erf,del})}(t_n - T_{\text{on}})\right].\end{aligned} \tag{18}$$

Equation (18)'s delayed signal from a chopped Gaussian beam is our model for the experimentally recorded signal. Its graph is shown in Fig. 2(C). Before fitting this model signal to experimental data, we add a background level B_0 in the model, because we see such a background in the data.

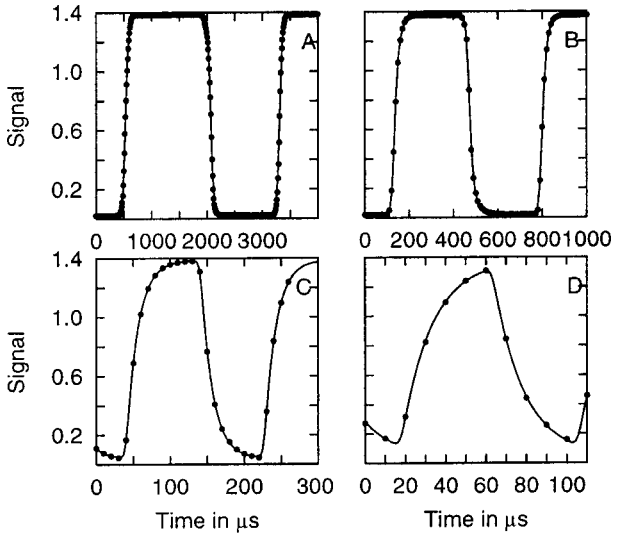

FIG. 3. Fits of $S^{(\text{erf,del})}(t)$ to recorded signal: (A) $f_{\text{chop}} \simeq 360$ Hz; (B) $f_{\text{chop}} \simeq 1.5$ kHz; (C) $f_{\text{chop}} \simeq 5.4$ kHz; and (D) $f_{\text{chop}} \simeq 11.4$ kHz.

V. TIME SERIES: DATA

Figure 3 shows the fit of $S^{(\text{erf,del})}(t)$ to a time series taken with various chopper frequencies. We fitted one pulse, and the decrease and increase of its neighboring pulses, with $S^{(\text{erf,del})}(t)$ in Eq. (18). The sum in Eq. (18) was truncated to include only terms that contribute in the finite time interval in question. In Fig. 3(A) the symmetric error-function profiles are seen, because σ_t is much larger than the response time τ. In Fig. 3(D), on the other hand, the opposite is the case: the slow response of the diode entirely dominates the form of the signal. The model signal in Eq. (18) is shown as a solid line in Fig. 3, and fits the data very well at all frequencies shown.

Some of the fitting parameters, or combinations of them, are plotted versus chopper frequency in Fig. 4. The delay time τ [panel (B)], the amplitude S_0 [panel (D)], and the ratio between the on and off times $T_{\text{on}}/T_{\text{off}}$ [panel (E)], are approximately independent of chopper frequency over the entire frequency range, as expected.

The two remaining parameters are difficult to determine precisely for all chopper frequencies investigated. The time σ_t that it takes the shutter to traverse approximately half the beam is only resolved well experimentally at low chopper frequencies, where the rise and fall of the signal is dominated by it. This is also illustrated by the nearly constant value for $\sigma_t/(T_{\text{on}} + T_{\text{off}})$ for chopper frequencies below 2–3 kHz, shown in Fig. 4(A).

The fraction $\alpha^{(\text{diode})}$ of instantaneous response of the diode cannot be determined at small chopper frequencies. Actually, it is not well determined at any of the frequencies investigated in our chopper experiments as its effect on the recorded signal is visible mainly for frequencies well above $1/(2\pi\tau)$. In our case, this frequency is about 8–9 kHz close to our maximum chopper frequency of 13.5 kHz.

As for the dependence on laser intensity, note that the amplitude S_0 is proportional to the intensity, the value of τ depends on it, the value of $\alpha^{(\text{diode})}$ does not, while the ratios

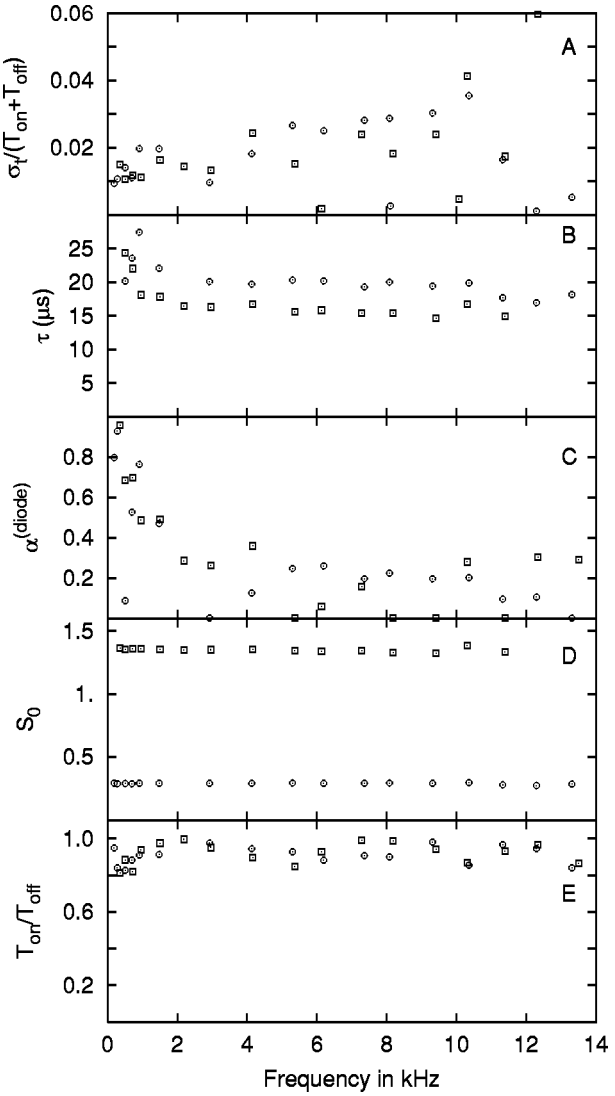

FIG. 4. Fitting parameters, or combinations of them, as functions of chopper frequency. Circles denote the values found at the lowest laser intensity used I_{low} and squares the values found at the largest intensity $I_{high} \simeq 4I_{low}$: (A) $\sigma_t/(T_{on}+T_{off})$; (B) characteristic time τ of diode's delayed response; (C) fraction $\alpha^{(diode)}$ of signal that causes instantaneous response in the diode; (D) signal amplitude S_0 of unchopped laser beam; and (E) the ratio of on to off time T_{on}/T_{off}.

T_{on}/T_{off} and $\sigma_t/(T_{on}+T_{off})$ do not and should not, because they only depend on the geometrical properties of the chopper wheel and laser beam.

VI. POWER SPECTRA

The good fits of the theory to the recorded time series vouch for this simple theory. The theory also gives an analytical form for the characteristic function that describes the filtering effect of the photodetection system. We find this function below, but first show that it can also be measured experimentally with precision, by power spectral analysis of the whole recorded time series.

The power spectrum of a periodic signal vanishes except at frequencies $f_k \equiv k/T$, where k is an integer and T is the period of the signal. In our case $T=1/f_{chop}$, so $f_k = k\, f_{chop}$. The power P_k located at the frequencies f_k is found by Fourier transforming one period of the signal

$$\tilde{S}_k \equiv T^{-1} \int_0^T dt\, S(t)\, e^{i2\pi f_k t}, \tag{19}$$

and using that

$$P_k \equiv \langle |\tilde{S}_k|^2 \rangle. \tag{20}$$

The normalizations chosen in Eqs. (19) and (20) are important, as they keep formulas below simpler. With these normalizations, the power spectrum that one would measure if one could record a perfectly periodic signal for infinite time would be

$$P(f) = \sum_k P_k \delta(f - f_k). \tag{21}$$

In the case where the periodic signal is produced by a chopper, the power P_k does not depend on the chopper frequency. Only the location on the frequency axis of this power depends on chopper frequency. The reason for this is that a change in chopper frequency does not change the amplitude of the light impinging on the diode in the periods when it is on, nor does it change the integrated time that the light is on within a fixed time interval. Only the frequency with which it turns on/off depends on f_{chop}. Phrased mathematically, the power P_k does not depend on the chopper frequency because the signal can be written

$$S(t) = s(t\, f_{chop}) = s(t/T), \tag{22}$$

where s is a periodic function with period one and defined by the chopper wheel's geometry and the beam's intensity profile, as exemplified below. Inserting this in Eq. (19), and using $f_k = k/T$, one finds

$$\tilde{S}_k = \int_0^1 d\xi\, s(\xi)\, e^{i2\pi k\xi}, \tag{23}$$

which clearly does not depend on f_{chop}. Neither does P_k then.

Specifically, the Fourier transform of the train of rectangular pulses resulting from chopping an infinitely narrow beam, Eq. (13), is

$$\tilde{S}_k^{(rect)} = \frac{S_0}{2}[1 - \exp(i2\pi ka)]\frac{i}{\pi k}, \tag{24}$$

hence

$$P_k^{(rect)} = \frac{S_0^2}{2\pi} \frac{1 - \cos(2\pi ka)}{k^2}, \tag{25}$$

where we have introduced the ratio $a = T_{on}/T$ of on time to period, a geometrical property of the chopper wheel, and approximately equal to 0.5 for our wheel, according to Fig. 4(E).

Similarly, the power spectrum of the chopped Gaussian beam profile is found by Fourier transforming the smoothed rectangular pulses of Eq. (16) to find

$$\tilde{S}_k^{(\mathrm{erf})} = \frac{S_0}{2}[1-\exp(i2\pi ka)]\frac{i}{\pi k}\exp[-2(\pi kc)^2], \quad (26)$$

hence

$$P_k^{(\mathrm{erf})} = \frac{S_0^2}{2\pi}\frac{1-\cos(2\pi ka)}{k^2}\exp[-(2\pi kc)^2], \quad (27)$$

where $c=\sigma_t/T=\sigma_x n_{\mathrm{hole}}/(2\pi r)$ is the ratio between the half width of the beam profile σ_x and the distance between chopper holes $2\pi r/n_{\mathrm{hole}}$. This ratio is small, 0.01–0.02 according to Fig. 4(A), but enters Eq. (27) with a factor $2\pi k$, and cuts off P_k with a Gaussian function of k.

As is well known in signal processing, the finite response time changes the power spectrum of a signal multiplicatively, by a characteristic function $|\tilde{g}(f)|^2$ depending on the delay function $g(t)$

$$P^{(\mathrm{del})}(f) = \langle|\tilde{S}^{(\mathrm{del})}(f)|^2\rangle = \langle|\tilde{S}*g(f)|^2\rangle$$
$$= \langle|\tilde{g}(f)\cdot\tilde{S}(f)|^2\rangle = |\tilde{g}(f)|^2 P(f). \quad (28)$$

Thus

$$P_k^{(\mathrm{del})}(f_{\mathrm{chop}}) = |\tilde{g}(k\,f_{\mathrm{chop}})|^2 P_k. \quad (29)$$

On the right-hand side of Eq. (29), f_{chop} occurs only in the characteristic function, while P_k is independent of f_{chop}. Consequently, the characteristic function can be determined experimentally by measuring the power $P_1^{(\mathrm{del})}(f_{\mathrm{chop}})$ at various chopper frequencies, and using

$$|\tilde{g}(f_{\mathrm{chop}})|^2 \propto P_1^{(\mathrm{del})}(f_{\mathrm{chop}}). \quad (30)$$

The constant of proportionality is determined by $|\tilde{g}(0)|^2=1$, i.e., it is $1/P_1^{(\mathrm{del})}(f_{\mathrm{chop}}\to 0)$. Here, $P_1^{(\mathrm{del})}(f_{\mathrm{chop}}\to 0)$ is best determined by fitting experimental results for $P_1^{(\mathrm{del})}(f_{\mathrm{chop}})$ with the theoretical characteristic function given below times a constant. Once fitted, this constant is $P_1^{(\mathrm{del})}(f_{\mathrm{chop}}\to 0)$.

The Fourier transform of the diode response function in Eq. (10) is

$$\tilde{g}(f) = \alpha^{(\mathrm{diode})} + \frac{1-\alpha^{(\mathrm{diode})}}{1-i2\pi f\tau}, \quad (31)$$

and the theoretical characteristic function is consequently

$$|\tilde{g}(f)|^2 = \alpha^{(\mathrm{diode})2} + \frac{1-\alpha^{(\mathrm{diode})2}}{1+(2\pi\tau f)^2}. \quad (32)$$

Note how $\alpha^{(\mathrm{diode})}$ occurs only squared in the characteristic function. If, as found below, 30% of the *signal* is registered instantaneously, then $\alpha^{(\mathrm{diode})}=0.30$. Consequently, $\alpha^{(\mathrm{diode})2}=0.09$, so only 9% of the *power* in the signal is registered unfiltered, while 91% occurs as filtered with a Lorentzian characterizing the filter.

VII. PHASE DRIFT, WINDOWING, LEAKAGE, AND WINDOW FUNCTIONS

In practice, a chopper does not give a perfectly periodic signal. Its frequency drifts a little with time. The dominant consequence is not the change in frequency itself, but the phase drift it causes: a slight change in frequency adds up to a significant change in phase after many cycles. If one Fourier transforms a signal with drifting phase, contributions with different phases partially cancel each other, and one gets the power spectrum wrong. Thus, finding P_k from experimental data is nontrivial.

The presence or absence of phase drift is easily diagnosed by plotting the signal as a function of time t modulo a period T. If there is no phase drift, T can be chosen as the signal's period, with the result that the graph of the signal collapses upon itself. If there is phase drift, this is seen as no such collapse being possible for cycles far separated in time, when the collapse occurs for cycles close to each other in time.

The remedy against power loss caused by phase drift is windowing: We break a signal which was recorded over a long time into many signals of shorter duration T_{window} so short that virtually no phase drift occurs in any one signal. How short that needs to be is easily diagnosed, as described in the previous paragraph.

Next we compute the power spectrum for each of these signals of duration T_{window}, and average these spectra to increase precision. Thus power loss due to phase drift is avoided.

However, since we work with signals of finite duration T_{window} the resulting power spectrum is known only at a discrete set of frequencies n/T_{window}, where n is an integer, and these frequencies typically do not coincide with the frequencies $f_k=k\,f_{\mathrm{chop}}$, k integer. The power located at f_k consequently *leaks* to neighboring frequencies n/T_{window}, making *leakage* an important issue for the present analysis.[28]

Fourier transforming as just described, using no special window function, amounts to using a rectangular window; see Ref. 28. Consequently, instead of $\tilde{S}_k$, Fourier transformation gives

$$\tilde{S}_n^{(\mathrm{rect})} = \frac{\sin(\pi kT_{\mathrm{window}}/T)}{\pi T_{\mathrm{window}}}\frac{\tilde{S}_k}{n/T_{\mathrm{window}}-k/T}, \quad (33)$$

so instead of the power spectral density $P(f)$ one finds

$$P_n^{(\mathrm{rect})} = \left|\sum_k \frac{\sin(\pi kT_{\mathrm{window}}/T)}{\pi T_{\mathrm{window}}}\frac{\tilde{S}_k}{n/T_{\mathrm{window}}-k/T}\right|^2. \quad (34)$$

In Fig. 5(A) this theoretical expression for the experimental power spectrum with leakage is compared with the actual experimental power spectrum computed with a rectangular window. The theoretical spectrum was obtained with Eqs. (26), (28), and (31), and the parameters found in Sec. IV. Good agreement is observed. The spectrum differs a good deal from the theoretical delta-function spectrum in Eq. (21), however. Leakage is significant with the rectangular window, as is well known, and basically converts delta functions to poles of second order. Leakage conserves power, however, so $P_1^{(\mathrm{del})}$ could be found experimentally from Fig. 5(A) if the area under the curve describing the pole at $f_1=f_{\mathrm{chop}}$ in Fig. 5(A) could be determined. That done, $P_1^{(\mathrm{del})}$'s dependence on f_{chop} could be measured experimentally and used in Eq. (30).

It is, however, more convenient to replace the rectangular window with any window that suppresses leakage, in or-

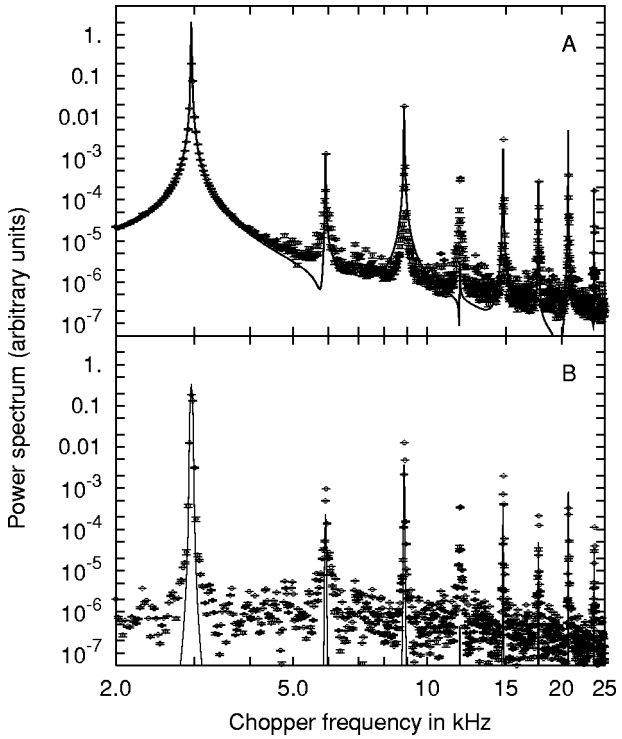

FIG. 5. Experimental power spectra shown as open circles with error bars. The laser intensity was at I_{high} and the chopper-frequency approximately 3 kHz. (A) Spectrum obtained with rectangular windows. Our model for this spectrum, [Eq. (34)], is shown as a full line. (B) Spectrum obtained with Hanning windows. Our model for this spectrum is shown as a full line. (This last model is not used, hence not given in this article.)

der to separate the peaks corresponding to different values of $f_k = k\, f_{\text{chop}}$ better. This has been done with a Hanning window in Fig. 5(B). Then the power $P_1^{(\text{del})}(f_{\text{chop}})$ associated with the peak at $f_1 = f_{\text{chop}}$ is more easily found. This is done by summing the few values of $P_n^{(\text{Hann})}$ near $n/T_{\text{window}} \sim f_{\text{chop}}$ that exceed 10^{-3} times the maximal value for $P_n^{(\text{Hann})}$ near f_{chop}.

VIII. RESULTS: DETECTION SYSTEM'S CHARACTERISTICS

We measured the characteristic function $|\tilde{g}(f)|^2$ experimentally by measuring $P_1^{(\text{del})}(f_{\text{chop}})$ as described in the previous paragraph, and using Eq. (30). Figure 6 shows a plot of our results, obtained at two different laser intensities. Fits to the data of the analytical expression for the characteristic function, [Eq. (32)] are also shown, as the full and dashed curves through the data points. The expression in Eq. (32) was fitted to the data only after we had multiplied it with the two characteristic functions of the two electronic filters built into our equipment. These functions are of the form given in Eq. (1), with $f_{3\text{dB}} = 50$ and 80 kHz, respectively.

The quality of the fits is not surprising, as we already fitted the signal in the time domain. We did that over only one period, however, while Fig. 6 shows a fit to data accumulated over thousands of periods. Thus the fits verify our theory for $|\tilde{g}(f)|^2$ and allow us to conclude again that the diode is well approximated by a first-order filter plus a small unfiltered response.

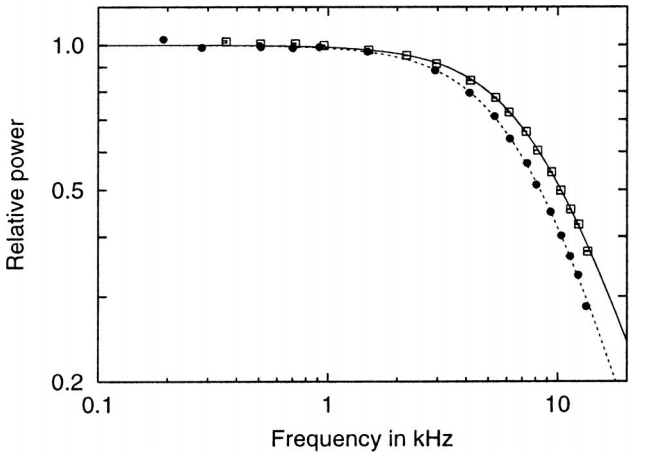

FIG. 6. Fraction of impinging power detected by the photodiode as a function of frequency. Data are shown for two experiments with different laser intensities: I_{high} shown with squares and $I_{\text{low}} \simeq I_{\text{high}}/4$ shown with circles. The solid and dashed lines are fits to the data of the theoretical characteristic function in Eq. (32), after electronic filters have been accounted for.

The parameter values determined by the two fits in Fig. 6 are given in Table I, with $f_{3\text{dB}}^{(\text{diode})} \equiv 1/(2\pi\tau)$. The tabulated values for $\alpha^{(\text{diode})}$ are seen to agree with those plotted in Fig. 4(C) with $f > 0.5$ kHz. The tabulated values for $f_{3\text{dB}}^{(\text{diode})}$ are seen to agree with the tabulated values for $1/(2\pi\tau_{\text{av}})$, with the values obtained from the power spectrum having somewhat higher precision. Both methods discard some information, much in theory, less in practice, where noise and errors of various kinds impose limits: By fitting to only one period, as shown in Fig. 3, we ignore the information from all other periods also contained in our record. This information is used in the power spectrum, but in this case we only use the spectrum's dominant, lowest-frequency peak at f_{chop}, and ignore the smaller, but additional information contained in the peaks at $f_k = k\, f_{\text{chop}}$, $k = 2, 3, \ldots$.

IX. INTENSITY DEPENDENCE OF $f_{3\text{dB}}^{(\text{diode})}$: MORE LIGHT, LESS FILTERING

In Table I, $f_{3\text{dB}}^{(\text{diode})}$ increases with laser intensity, while $\alpha^{(\text{diode})}$ seems to, but this is not significant because of the relatively large errors on its values. Using Eq. (7), we have

$$f_{3\text{dB}}^{(\text{diode})} = \frac{\pi \mathcal{D}}{8L^2}. \tag{35}$$

So the reason $f_{3\text{dB}}^{(\text{diode})}$ increases with laser intensity could be that $\mathcal{D} = \mu k_B T$ does, μ being the mobility of holes[29], k_B

TABLE I. Second and third column: Fitting parameters obtained by fitting Eq. (32) to data as shown in Fig. 6. Fourth column: $1/(2\pi\tau_{\text{av}})$ with τ_{av} the average value of τ for chopper frequencies between 2 and 12 kHz in Fig. 4(B). Values in the third and fourth columns agree within errors, but results obtained with power spectral analysis (third column) are the more precise. $I_{\text{high}} \simeq 4 I_{\text{low}}$.

Intensity	$\alpha^{(\text{diode})}$	$f_{3\text{dB}}^{(\text{diode})}$ (kHz)	$1/(2\pi\tau_{\text{av}})$ (kHz)
I_{low}	0.3 ± 0.1	7.9 ± 0.2	8.1 ± 0.3
I_{high}	0.4 ± 0.1	9.3 ± 0.2	10.1 ± 0.5

Boltzmann's constant, and T the absolute temperature, which might increase with laser intensity if the diode is heated by absorbed light. This explanation is easily excluded, as μ is known to *decrease* with temperature, theoretically as $T^{-3/2}$ due to lattice scattering, experimentally approximately as $T^{-2.5}$ at room temperature (Ref. 27, Sect. 4.5b). So $\mathcal{D}$ actually decreases with increasing temperature.

A decrease in L with increasing laser intensity is a more realistic explanation. If the depletion layer's thickness $L^{(\mathrm{dep})}$ increases with increased photovoltaic loading of the diode, L would decrease by the same amount. An 8% decrease in L would account for Table I's increase in $f_{3\mathrm{dB}}^{(\mathrm{diode})}$ with laser intensity. A decrease in L is known to occur with increased reverse bias voltage, and we have observed $f_{3\mathrm{dB}}^{(\mathrm{diode})}$ increase significantly with it.

Equation (12) gives $\alpha^{(\mathrm{diode})}$ as function of $L/(L^{(\mathrm{dep})}+L)$. Here $L^{(\mathrm{dep})}+L$ is a constant, the thickness of the photodiode (320 μm in our case) when we neglect the thickness <1 μm of the p-layer. Using Eq. (35) to eliminate L in favor of $f_{3\mathrm{dB}}^{(\mathrm{diode})}$, we find

$$\alpha^{(\mathrm{diode})} = 1 - \sqrt{\frac{8\mathcal{D}}{\pi^3 (L^{(\mathrm{dep})}+L)^2}},$$

$$= 1 - \sqrt{\frac{3.3\,\mathrm{kHz}}{f_{3\mathrm{dB}}^{(\mathrm{diode})}}}. \tag{36}$$

Insertion of the values for $f_{3\mathrm{dB}}^{(\mathrm{diode})}$ listed in Table I gives $\alpha^{(\mathrm{diode})}(I_{\mathrm{low}}) = 0.35(1)$ and $\alpha^{(\mathrm{diode})}(I_{\mathrm{high}}) = 0.40(1)$, in perfect agreement with the measured values.

Again using the values for $f_{3\mathrm{dB}}^{(\mathrm{diode})}$ given in Table I, we find from Eq. (35) that $L(I_{\mathrm{low}}) = 253\,\mu$m and $L(I_{\mathrm{high}}) = 233\,\mu$m, which does not conflict with $L^{(\mathrm{dep})}+L = 320\,\mu$m. Consequently, we have $L^{(\mathrm{dep})}(I_{\mathrm{low}}) = 67\,\mu$m and $L(I_{\mathrm{high}}) = 87\,\mu$m, which seems high compared to the values given in Fig. 1, but then we do not know how the depletion layer is affected when the diode is illuminated, and the boundary between the depletion layer and the n-layer is not sharp, as we have treated it here, so we should expect some error on our values for L and $L^{(\mathrm{dep})}$.

Whatever the reason for the variability of $f_{3\mathrm{dB}}^{(\mathrm{diode})}$, both values in Table I are low, 8–9 kHz, to be compared with $f_{3\mathrm{dB}} = 50$ and 80 kHz for the built-in electronic filters. Thus the diode is the dominant low-pass filter in the setup. This is important to take into account in experiments using a 1064 nm laser in connection with a Si PIN photodiode. A theory for how $f_{3\mathrm{dB}}^{(\mathrm{diode})}$ depends on the intensity of light falling on the diode is of little practical value, however, because this intensity is unknown. Instead, one must recalibrate the diode each time this intensity is changed. To this end it is very practical to know its characteristic function's form, as established here.

X. CONCLUSIONS

We have demonstrated a substantial frequency-dependence and corresponding power-loss of a generic photodetection system based on a Si PIN photodiode in connection with a 1064 nm laser, a system often used, e.g., in optical tweezer setups. We propose to use a simple mechanical chopper to diagnose this power loss, and to account for it by determining its characteristics. Instead of a chopper, one may use an acousto-optical deflector.

Our results show that the power lost in the photodiode's "filter" depends on the impinging laser intensity, with less power lost for higher intensities. This dependence on intensity makes it necessary to fit $f_{3\mathrm{dB}}^{(\mathrm{diode})}$ and $\alpha^{(\mathrm{diode})}$ anew in each experiment in which one wants to take this effective filter into account.

We see four possible solutions to this problem: (i) Find a diode that is better suited for infrared laser light. InGaAs diodes may be a better choice, but they have other shortcomings; so far they are available only in small sizes, and some of them need to be cooled to work as desired for the appropriate laser intensities. (ii) Another solution is to measure the characteristic function as described here, and take it into account when interpreting results. This approach is feasible only when the intensity of laser light impinging on the diode can be arranged to be the same during calibration and experiment. (iii) When this is not the case, one must calibrate *during* the experiment itself, if possible. In the case of optical tweezers, Ref. 15 describes how this can be done using not a chopper, but the Brownian motion of a bead in the optical trap, to produce rapid changes in the light hitting the diode. (iv) Since $f_{3\mathrm{dB}}^{(\mathrm{diode})}$ also depends on the reverse bias voltage through the width of the depletion layer, $f_{3\mathrm{dB}}^{(\mathrm{diode})}$ can be increased significantly by increasing this voltage. That, however, increases the noise level. So there is a tradeoff, and calibration may be preferable, now that the known form of the characteristic function makes it possible. The calibration we did here with zero reverse bias voltage represents the extremal case of highest power loss. Calibration with finite reverse bias voltage consequently is a simpler task.

ACKNOWLEDGMENTS

We thank Jakob Kisbye Dreyer for technical assistance, and Thomas Brosowski (Pacific Silicon Sensor, Berlin), Lars Koldbæk (Hamamatsu Photonics, Denmark), Wolfgang Öffner (EMBL-Heidelberg), Per Hedegård, Kilian Singer, and Selim Joachim for helpful correspondences and discussions. This work was financially supported by the Danish Research Agencies.

[1] G. Meyer and N. M. Amer, Appl. Phys. Lett. **53**, 1045 (1988).
[2] S. Alexander, L. Hellemans, O. Marti, J. Schneir, V. Elings, P. K. Hansma, M. Longmire, and J. Gurley, J. Appl. Phys. **65**, 164 (1989).
[3] A. D. Mehta, J. T. Finer, and J. A. Spudich, Methods Cell Biol. **55**, 47 (1998).
[4] F. Gittes and C. F. Schmidt, Opt. Lett. **23**, 7 (1998).
[5] G. Lutz, Semiconductor Radiation Detectors (Springer, Berlin, 1999).
[6] C. Yang, D. N. Jamieson, S. M. Hearne, C. I. Pakes, B. Rout, E. Gauja, A. J. Dzurak, and R. G. Clark, Nucl. Instrum. Methods Phys. Res. B **190**, 212 (2002).
[7] S. B. Smith, Y. Cui, and C. Bustamante, Science **271**, 795 (1996).
[8] M. D. Wang, M. J. Schnitzer, H. Yin, R. Landick, J. Gelles, and S.M. Block, Science **282**, 902 (1998).
[9] C. Veigel, M. L. Bartoo, D. C. W. White, J. C. Sparrow, and J. E. Molloy, Biophys. J. **75**, 1424 (1998).
[10] C. Veigel, L. M. Coluccio, J. D. Jontes, J. C. Sparrow, R. A. Milligan, and J. E. Molloy, Nature (London) **398**, 530 (1999).

[11] M. J. Schnitzer, K. Visscher, and S. M. Block, Nature Cell Biology, **2**, 718 (2000).
[12] J.-C. Meiners and S. R. Quake, Phys. Rev. Lett. **84**, 5014 (2000).
[13] D. E. Smith, S. J. Tans, S. B. Smith, S. Grimes, D. L. Anderson, and C. Bustamante, Nature (London) **413**, 748 (2001).
[14] M. J. Lang, C. L. Asbury, J. W. Shaevitz, and S. M. Block, Biophys. J. **83**, 491 (2002).
[15] K. Berg-Sørensen and H. Flyvbjerg, Phys. Rev. Lett. (submitted).
[16] F. Gittes, B. Schnurr, P. D. Olmsted, F. C. MacKintosh, and C. F. Schmidt, Phys. Rev. Lett. **79**, 3286 (1997).
[17] A. Pralle, E.-L. Florin, E. H. K. Stelzer, and J. K. H. Hörber, Appl. Phys. A: Mater. Sci. Process. **66**, S71 (1998).
[18] E.-L. Florin, A. Pralle, E. H. K. Stelzer, and J. K. H. Horber, Appl. Phys. A: Mater. Sci. Process. **66**, S75 (1998).
[19] A. Pralle, M. Prummer, E.-L. Florin, E. H. K. Stelzer, and J. K. H. Horber, Microsc. Res. Tech. **44**, 378 (1999).
[20] A. Pralle, P. Keller, E.-L. Florin, K. Simons, and J. K. H. Horber, J. Cell Biol. **148**, 997 (2000).
[21] E. Helfer, S. Harlepp, L. Bourdieu, J. Robert, F. C. MacKintosh, and D. Chatenay, Phys. Rev. Lett. **85**, 457 (2000).
[22] E. Helfer, S. Harlepp, L. Bourdieu, J. Robert, F. C. MacKintosh, and D. Chatenay, Phys. Rev. E **63**, 021904 (2001).
[23] Si PIN photodiode S5980, S5981, S5870. Cat. No. KPIN1012E02, April 2001.
[24] Photodiodes. Cat. No. KPD0001E07, 1998.
[25] S. M. Sze. Physics of Semiconductor Devices (J Wiley, New York, 1981).
[26] N. W. Ashcroft and N. D. Mermin, Solid State Physics Holt-Saunders Int'l. ed. (Saunder's College Press, Philadelphia, PA, 1981).
[27] A. S. Grove. Physics and Technology of Semiconductor Devices (Wiley, New York, 1967).
[28] W. H. Press, B. P. Flannery, S. A. Teukolsky, and W. T. Vetterling, Numerical Recipes. (Cambridge University Press, Cambridge, 1986).
[29] One should not confuse this, the mobility of holes, with the electrical conductivity, often denoted by the same letter. The electrical conductivity increases dramatically with temperature, because the number of charge carriers does, much more than their mobility drops (Ref. 26).